

Is There News in Inventories?*

ONLINE APPENDIX

Christoph Görtz
University of Birmingham[†]

Christopher Gunn
Carleton University[‡]

Thomas A. Lubik
Federal Reserve Bank of Richmond[§]

May 2020

*The views expressed in this paper are those of the authors and not necessarily those of the Federal Reserve Bank of Richmond or the Federal Reserve System.

[†]Department of Economics. University House, Birmingham B15 2TT. United Kingdom. Tel.: +44 (0) 121 41 43279. Email: c.g.gortz@bham.ac.uk

[‡]Department of Economics. Loeb Building, 1125 Colonel By Drive. Ottawa, ON, K1S 5B6. Canada. Tel.: +1 613 520 2600x3748. Email: chris.gunn@carleton.ca.

[§]Research Department, P.O. Box 27622, Richmond, VA 23261. Tel.: +1-804-697-8246. Email: thomas.lubik@rich.frb.org.

A Additional VAR Evidence

A.1 Forecast Error Variance Decomposition

Figure 1 reports the forecast error variance decomposition for our baseline specification in the main text. It shows the variance shares explained by the TFP news shock over a 40-period (10-year) time horizon. In the long run, the news shock explains about 50% of TFP fluctuations, the remainder being due to unanticipated movements in productivity. For all other quantity variables the contribution of TFP news is above 50%, with the contribution of GDP at around three quarters. This is consistent with the findings in the literature which attribute similar importance to anticipated TFP movements.

A.2 News Shocks and the Response of Inventories over a Longer Sample Period

It has been widely documented in the literature (for instance, McCarthy and Zakrajsek, 2007) that changes in the behavior of inventories coincide with the onset of the Great Moderation in the early 1980s. It is this observation, in addition to data availability issues that we highlight in the main text, that we and most of the literature focus on a post-Great Moderation sample. Nevertheless, it is interesting to evaluate whether the rise of inventories in anticipation of higher future TFP is present also over a longer horizon.

Figure 2 shows the impulse responses for the 1960Q1- 2018Q2 sample period, computed using the same news shock identification procedure as in the baseline. The individual graphs reveal strong comovement of all macroeconomic aggregates, including inventories, several quarters before TFP increases significantly. This sample is restricted by the availability of the E5Y consumer confidence measure. Using the S&P500 stock index in its place we can consider a 1948Q1-2018Q2 sample.

Figure 3 shows that responses to a news shock based on this sample are qualitatively and also largely quantitatively very similar to the results based on our 1983Q1- 2018Q2 baseline sample and the 1960Q1-2018Q2 sample period. Overall, we find that the fact that inventories rise in response to a TFP news shock is robust at longer sample periods.

A.3 Robustness to Alternative VAR News Shock Identification

In our baseline specification, we identify news shocks using the Max Share method proposed by Francis et al. (2014). This approach is widely used in the literature; it identifies a news shock as the shock that (i) does not move TFP on impact, and (ii) maximizes the variance

of TFP at a 40-quarter horizon. We assess the robustness of our findings using three closely related alternative approaches.

First, we consider the identification scheme suggested by Barsky and Sims (2011). Their method recovers a news shock by maximizing the variance of TFP over horizons from zero to 40 quarters and the restriction that the news shock does not move TFP on impact. The second alternative identification scheme is Forni et al. (2014), which is similar in spirit to the Max Share method. They identify the news shock by imposing a zero-impact restriction on TFP and maximize the impact of the shock on TFP in the long run. Third, we use identification suggested by Kurmann and Sims (2019), who recover news shocks by maximizing the forecast error variance of TFP at a long horizon without imposing a zero-impact restriction on TFP conditional on the news shock.¹

Figure 4 provides a comparison between the median responses based on the Max Share method and the methods proposed by Barsky and Sims (2011) and Forni et al. (2014). The median responses of the Max Share methodology and the Forni et al. (2014) methodology are virtually indistinguishable. In turn, both are very similar to the median responses based on the Barsky and Sims (2011) approach. Figure 5 shows that responses based on the methodology proposed by Kurmann and Sims (2016) are qualitatively and quantitatively close to the ones based on the Max-share method. Perhaps most importantly, all methods suggest inventories increase in anticipation of higher future TFP.

A.4 News Shock Identification Based on Patents

We also consider as a robustness exercise identification of news shocks that relies on value-weighted patents. In this we follow the idea in Cascaldi-Garcia and Vukotic (2019) who argue that patent filings include information about future TFP movements since firms engage in activities to take advantage of expected technological improvements or are the originators of such productivity advancements. The patent system is designed to reveal such news without the full set of improvements necessarily being in place.

Kogan et al. (2017) use observations on patents associated with stockmarket listed firms in the CRSP database. They compute the economic value of a patent based on a firm's stock-price reaction to observed news about a patent grant, controlling for factors that could move stock prices but are unrelated to the economic value of the patent. Kogan et al. (2017) provide an annual index, while Cascaldi-Garcia and Vukotic (2019) use the associated micro data to aggregate to a quarterly index. They then use this index to identify responses to

¹Kurmann and Sims (2019) argue that allowing TFP to jump freely on impact, conditional on a news shock, produces robust inference to cyclical measurement error in the construction of TFP.

patent-based news shocks in a Bayesian VAR based on a simple Cholesky identification with the patent series ordered first.

Figure 6 shows impulse response functions to this patent-based news shock. They are broadly consistent with the responses in the baseline setup. TFP rises significantly only with a delay, even though there is no zero-impact restriction applied. Inventories rise on impact together with the other activity variables as well as consumer confidence. Unfortunately, the availability of the Kogan et al. (2017) value-weighted patents series restricts the sample to end in 2010Q4, while at the same time the composition of the index is limited to stockmarket-listed firms only. Nevertheless, the qualitative consistency of responses to a patent-based news shock with our baseline results is reassuring since the identification of the former is independent of the observable for TFP.

B DSGE Model Equations

The DSGE model introduced in section 3 of the main text is described by a set of optimality conditions. They define a symmetric competitive equilibrium as a set of stochastic processes $\{C_t, I_t, G_t, S_t, Y_t, N_t, u_t, F_t, K_t, H_t, X_t, A_t, w_t, r_t, \tau_t, \mu_t^f, \mu_t^k, \mu_t^h, \lambda_t\}_t^\infty$. In the following, we list these equations and detail how to transform the non-stationary system, which is driven by stochastic trends, into a stationary counterpart amenable to solution and estimation.

B.1 Optimality Conditions

We define $V_t = C_t - \psi n_t^\xi F_t$ as the periodic utility function argument to ease notation. In addition, we denote μ_t^f , μ_t^k , μ_t^h , and λ_t as, respectively, the multipliers on the definition of F_t (equation (9) in the main text), physical capital accumulation (equation (10) in the main text), knowledge capital accumulation (equation (11) in the main text) and the household budget constraint (equation (12) in the main text). The first-order necessary conditions are then as follows:

$$C_t + \Gamma_t I_t + G_t = S_t, \quad (1)$$

$$F_t = C_t^{\gamma_f} F_{t-1}^{1-\gamma_f}, \quad (2)$$

$$K_{t+1} = [1 - \delta(u_t)] K_t + m_t I_t \left[1 - S \left(\frac{I_t}{I_{t-1}} \right) \right], \quad (3)$$

$$H_{t+1} = H_t^{\gamma_h} N_t^{\nu_h}, \quad (4)$$

$$G_t = \left(1 - \frac{1}{\varepsilon_t} \right) Y_t, \quad (5)$$

$$\Gamma_t V_t^\sigma + \mu_t^f \gamma_f \frac{F_t}{C_t} = \lambda_t, \quad (6)$$

$$\xi \psi \Gamma_t V_t^{-\sigma} N_t^{\xi-1} F_t = \lambda_t w_t H_t + \mu_t^h \nu_h \frac{H_{t+1}}{N_t}, \quad (7)$$

$$r_t = \frac{\mu_t^k}{\lambda_t} \delta I(u_t), \quad (8)$$

$$\Upsilon_t \lambda_t = \mu_t^k m_t \left\{ 1 - S \left(\frac{I_t}{I_{t-1}} \right) - S' \left(\frac{I_t}{I_{t-1}} \right) \frac{I_t}{I_{t-1}} \right\} + \beta E_t \mu_{t+1}^k m_{t+1} S' \left(\frac{I_{t+1}}{I_t} \right) \left(\frac{I_{t+1}}{I_t} \right)^2, \quad (9)$$

$$\mu_t^f = -\psi \Gamma_t V_t^{-\sigma} N_t^\xi + \beta (1 - \gamma_f) E_t \mu_{t+1}^f \frac{F_{t+1}}{F_t}, \quad (10)$$

$$\mu_t^k = \beta E_t \left\{ \lambda_{t+1} r_{t+1} u_{t+1} + \mu_{t+1}^k [1 - \delta(u_{t+1})] \right\}, \quad (11)$$

$$\mu_t^h = \beta E_t \left\{ \lambda_{t+1} w_{t+1} N_{t+1} + \mu_{t+1}^h \gamma_h \frac{H_{t+2}}{H_{t+1}} \right\}, \quad (12)$$

$$Y_t = z_t (\Omega_t H_t N_t)^\alpha (u_t K_t)^{1-\alpha}, \quad (13)$$

$$w_t = \alpha \tau_t \frac{Y_t}{H_t N_t}, \quad (14)$$

$$r_t = (1 - \alpha) \tau_t \frac{Y_t}{u_t K_t}, \quad (15)$$

$$A_t = (1 - \delta_x) X_{t-1} + Y_t, \quad (16)$$

$$X_t = A_t - S_t, \quad (17)$$

$$\frac{\theta - 1}{\theta} = \beta (1 - \delta_x) E_t \frac{\lambda_{t+1}}{\lambda_t} \tau_{t+1}, \quad (18)$$

$$\tau_t = \frac{\zeta S_t}{\theta A_t} + \frac{\theta - 1}{\theta}. \quad (19)$$

In addition, we have laws of motion for the exogenous processes Γ_t , m_t , ϵ_t , $g_t^\Upsilon = \Upsilon_t / \Upsilon_{t-1}$ and $g_t^\Omega = \Omega_t / \Omega_{t-1}$ as described in the main text.

B.2 Stationarity and Solution Method

The model economy inherits stochastic trends from the two non-stationary stochastic processes for Υ_t and Ω_t . Our solution method focuses on isolating fluctuations around these stochastic trends. We divide non-stationary variables by their stochastic trend component to derive a stationary version of the model. We then take a linear approximation of the dynamics around the steady state of the stationary system.

The stochastic trend components of output and capital are given by $X_t^y = \Upsilon_t^{\frac{\alpha-1}{\alpha}} \Omega_t$ and $X_t^k = \Upsilon_t^{\frac{-1}{\alpha}} \Omega_t$, respectively. The stochastic trend components of all another non-stationary variables can be expressed as some function of X_t^y and X_t^k . In particular, define the following

stationary variables as transformations of the above 19 endogenous variables: $c_t = \frac{C_t}{X_t^y}$, $i_t = \frac{I_t}{X_t^y}$, $g_t = \frac{G_t}{X_t^y}$, $s_t = \frac{S_t}{X_t^y}$, $y_t = \frac{Y_t}{X_t^y}$, $n_t = N_t$, $u_t = u_t$, $f_t = \frac{F_t}{X_t^y}$, $k_t = \frac{K_t}{X_{t-1}^k}$, $h_t = H_t$, $x_t = \frac{X_t}{X_t^y}$, $a_t = \frac{A_t}{X_t^y}$, $\bar{w}_t = \frac{w_t}{X_t^y}$, $\bar{r}_t = \frac{X_t^k}{X_t^y} r_t$, $\tau_t = \tau_t$, $\bar{\mu}_t^f = (X_t^y)^\sigma \mu_t^f$, $q_t^k = \frac{X_t^k (\mu_t^k / \lambda_t)}{X_t^y}$, $q_t^h = \frac{\mu_t^h / \lambda_t}{X_t^y}$ and $\bar{\lambda}_t = (X_t^y)^\sigma \lambda_t$. In addition, define the two additional stationary variables, $g_t^y = \frac{X_t^y}{X_{t-1}^y}$ and $g_t^k = \frac{X_t^k}{X_{t-1}^k}$ as the growth-rates of the stochastic trends in output and capital, and $v_t = \frac{V_t}{X_t^y}$ as the definition of the stationary counterpart of the periodic utility function argument V_t defined above.

The stationary system is then given by:

$$c_t + i_t + g_t = s_t, \quad (20)$$

$$f_t = c_t^{\gamma_f} \left(\frac{f_{t-1}}{g_t^y} \right)^{1-\gamma_f}, \quad (21)$$

$$k_{t+1} = [1 - \delta(u_t)] \frac{k_t}{g_t^k} + m_t i_t \left[1 - S \left(\frac{i_t g_t^k}{i_{t-1}} \right) \right], \quad (22)$$

$$h_{t+1} = h_t^{\gamma_h} n_t^{\nu_h}, \quad (23)$$

$$g_t = \left(1 - \frac{1}{\varepsilon_t} \right) y_t, \quad (24)$$

$$\Gamma_t v_t^\sigma + \mu_t^f \gamma_f \frac{f_t}{c_t} = \bar{\lambda}_t, \quad (25)$$

$$\xi \psi \Gamma_t v_t^{-\sigma} n_t^{\xi-1} \frac{f_t}{\lambda_t} = \bar{w}_t h_t + q_t^h \nu_h \frac{h_{t+1}}{n_t}, \quad (26)$$

$$\bar{r}_t = q_t^k \delta'(u_t), \quad (27)$$

$$1 = q_t^k m_t \left\{ 1 - S \left(\frac{i_t g_t^k}{i_{t-1}} \right) - S' \left(\frac{i_t g_t^k}{i_{t-1}} \right) \frac{i_t g_t^k}{i_{t-1}} \right\} + \beta E_t g_{t+1}^\gamma (g_{t+1}^y)^{-\sigma} \frac{\bar{\lambda}_{t+1}}{\lambda_t} q_{t+1}^k m_{t+1} S' \left(\frac{i_{t+1} g_{t+1}^k}{i_t} \right) \left(\frac{i_{t+1} g_{t+1}^k}{i_t} \right)^2, \quad (28)$$

$$\bar{\mu}_t^f = -\psi \Gamma_t v_t^{-\sigma} n_t^\xi + \beta (1 - \gamma_f) E_t (g_{t+1}^y)^{1-\sigma} \bar{\mu}_{t+1}^f \frac{f_{t+1}}{f_t}, \quad (29)$$

$$q_t^k = \beta E_t g_{t+1}^\gamma (g_{t+1}^y)^{-\sigma} \frac{\bar{\lambda}_{t+1}}{\lambda_t} \left\{ \bar{r}_{t+1} u_{t+1} + q_{t+1}^k [1 - \delta(u_{t+1})] \right\}, \quad (30)$$

$$q_t^h = \beta E_t (g_{t+1}^y)^{-\sigma} \frac{\bar{\lambda}_{t+1}}{\lambda_t} \left\{ \bar{w}_{t+1} n_{t+1} + q_{t+1}^h \gamma_h \frac{h_{t+2}}{h_{t+1}} \right\}, \quad (31)$$

$$y_t = (h_t n_t)^\alpha \left(u_t \frac{k_t}{g_t^k} \right)^{1-\alpha}, \quad (32)$$

$$\bar{w}_t = \alpha \tau_t \frac{y_t}{h_t n_t}, \quad (33)$$

$$\bar{r}_t = (1 - \alpha) \tau_t \frac{y_t}{u_t \frac{k_t}{g_t^k}}, \quad (34)$$

$$a_t = (1 - \delta_x) \frac{x_{t-1}}{g_t^y} + y_t, \quad (35)$$

$$x_t = a_t - s_t, \quad (36)$$

$$\frac{\theta - 1}{\theta} = \beta(1 - \delta_x) E_t (g_{t+1}^y)^{-\sigma} \frac{\bar{\lambda}_{t+1}}{\bar{\lambda}_t} \tau_{t+1}, \quad (37)$$

$$\tau_t = \frac{\zeta s_t}{\theta z_t} + \frac{\theta - 1}{\theta}, \quad (38)$$

$$g_y^y = g_t^\Omega (g_t^\Upsilon)^{(\alpha-1)/\alpha}, \quad (39)$$

$$g_t^k = g_t^y / g_t^\Omega, \quad (40)$$

in addition to the exogenous processes Γ_t , m_t , ϵ_t , g_t^Υ and g_t^Ω .

C Shock Processes and Bayesian Estimation

To estimate the model, we include the following exogenous disturbances: a shock to the growth rate of TFP (g_y^y), a shock to the growth rate of IST (g_t^Ω), a marginal efficiency of investment (MEI) shock (m_t), a preference shock (Γ_t) and a government spending shock (ϵ_t). Each exogenous disturbance is expressed in log-deviations from the steady state as a first-order autoregressive process, whose stochastic innovation is uncorrelated with other shocks, has a zero mean, and is normally distributed. In addition to the unanticipated innovations to the above shocks, the model allows for anticipation effects. In particular, all shock processes (with the exception of the preference shock) include four, eight and twelve quarter-ahead innovations. Our treatment of anticipated and unanticipated components is standard and in line with the literature.²

We estimate the model over the period from 1983Q1 to 2018Q2, as in the VAR analysis. We use GDP, consumption, investment, inventories, and hours worked as observables. The variables are expressed in real per-capita terms as outlined in Section 2 in the main text, while GDP, consumption, investment, and inventories enter the vector of observables in first differences. We demean the data prior to estimation.

We only estimate the persistence parameters of the shocks and their standard deviations, while the remaining parameters shown in Table 1 in the main text are calibrated. The prior distributions follow the assumptions in Schmitt-Grohé and Uribe (2012). The prior means assumed for the news components are in line with these studies and imply that the sum

²For example Schmitt-Grohé and Uribe (2012) also include news components in the processes for government spending shocks and stationary as well as non-stationary neutral and investment-specific technology shocks. News shocks also arrive at the four, eight and twelve quarter-horizons as in Görtz et al. (2017), for example.

of the variance of news components is, evaluated at prior means, at most one half of the variance of the corresponding unanticipated component. Table A.1 provides an overview about prior and posterior distributions. Overall, the data are informative and indicate strong persistence in the MEI shock, but also in government spending. At the same time, TFP and IST growth exhibit a reasonably high degree in serial correlation, in line with the behavior of U.S. quantity variables such as GDP.

References

- [1] Barsky, Robert B., and Eric R. Sims (2011): “News shocks and business cycles”. *Journal of Monetary Economics*, 58(3), pp. 273-289.
- [2] Cascaldi-Garcia, Danilo, and Marija Vukotić (2019): “Patent-based news shocks”. Forthcoming, *Review of Economics and Statistics*.
- [3] Forni, Mario, Luca Gambetti, and Luca Sala (2014): “No news in business cycles”. *Economic Journal*, 124, pp. 1168-1191.
- [4] Francis, Neville, Michael Owyang, Jennifer Roush, and Riccardo DiCeccio (2014): “A flexible finite-horizon alternative to long-run restrictions with an application to technology shocks”. *Review of Economics and Statistics*, 96, pp. 638-647.
- [5] Görtz, Christoph, John Tsoukalas, and Francesco Zanetti (2017): “News shocks under financial frictions”. Technical Report.
- [6] Kogan, Leonid, Dimitris Papanikolaou, Amit Seru, and Noah Stockman (2017): “Technological innovation, resource allocation, and growth”. *Quarterly Journal of Economics*, 132(2), pp. 665-712.
- [7] Kurmann, Andre, and Eric Sims (2019): “Revisions in utilization-adjusted TFP and robust identification of news shocks”. Forthcoming, *Review of Economics and Statistics*.
- [8] McCarthy, Jonathan, and Egon Zakrajsek (2007): “Inventory dynamics and business cycles: What has changed?” *Journal of Money, Credit and Banking*, 39(2-3), pp. 591-613.
- [9] Schmitt-Grohé, Stephanie and Martín Uribe (2012): “What’s news in business cycles?” *Econometrica*, 80(6), pp. 2733-2764.

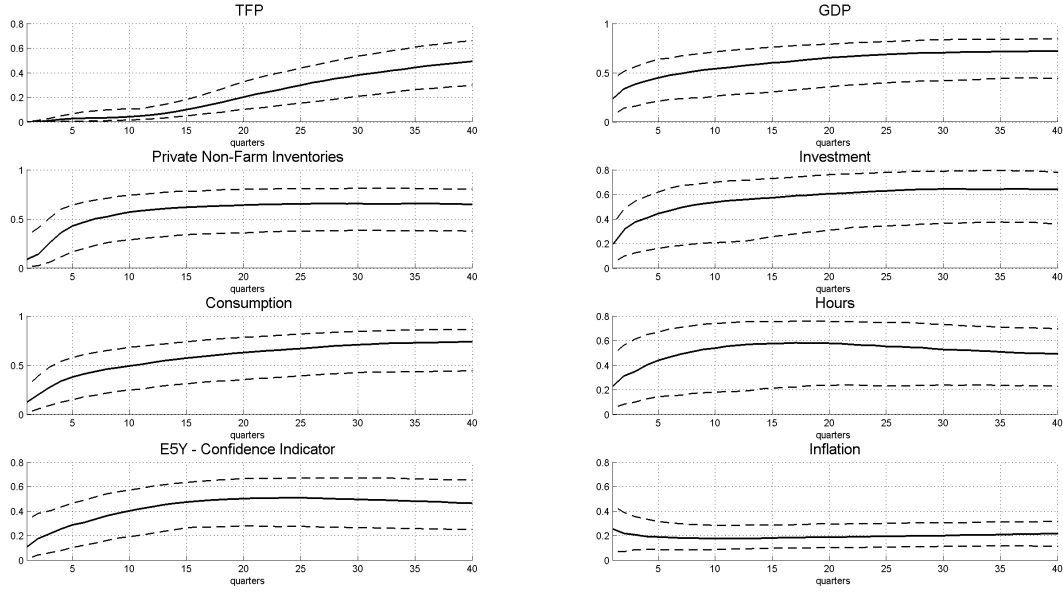


Figure 1: Forecast error variance decomposition (FEVD) of variables to the TFP news shock. Sample 1983Q1-2018Q2. The solid line is the median and the dashed lines are the 16% and 84% posterior bands generated from the posterior distribution of VAR parameters.

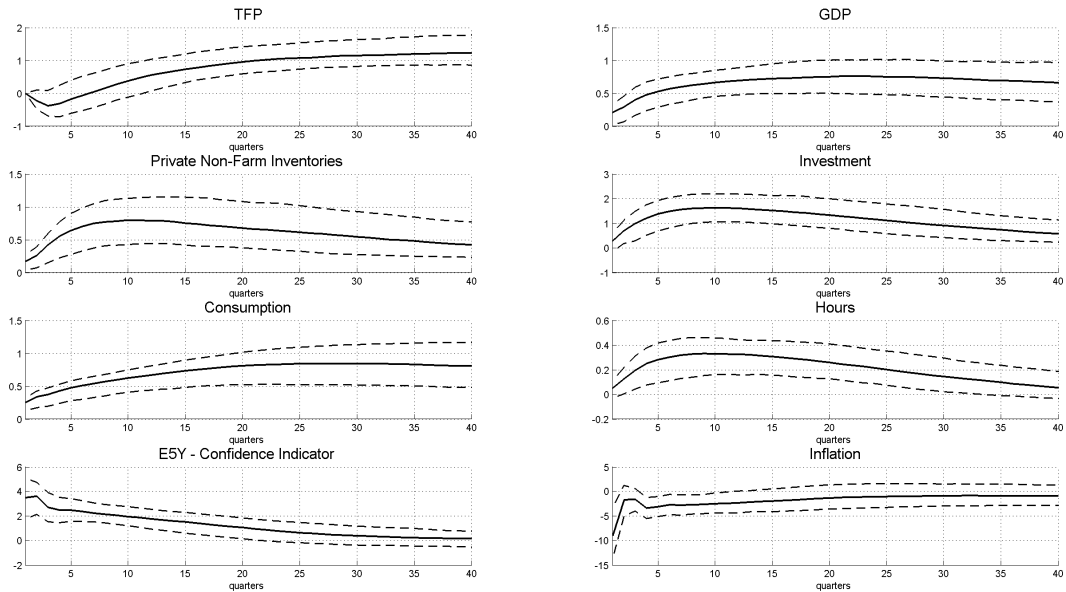


Figure 2: IRF to TFP news shock. Sample 1960Q1-2018Q2. The solid line is the median and the dashed lines are the 16% and 84% posterior bands generated from the posterior distribution of VAR parameters. The units of the vertical axes are percentage deviations.

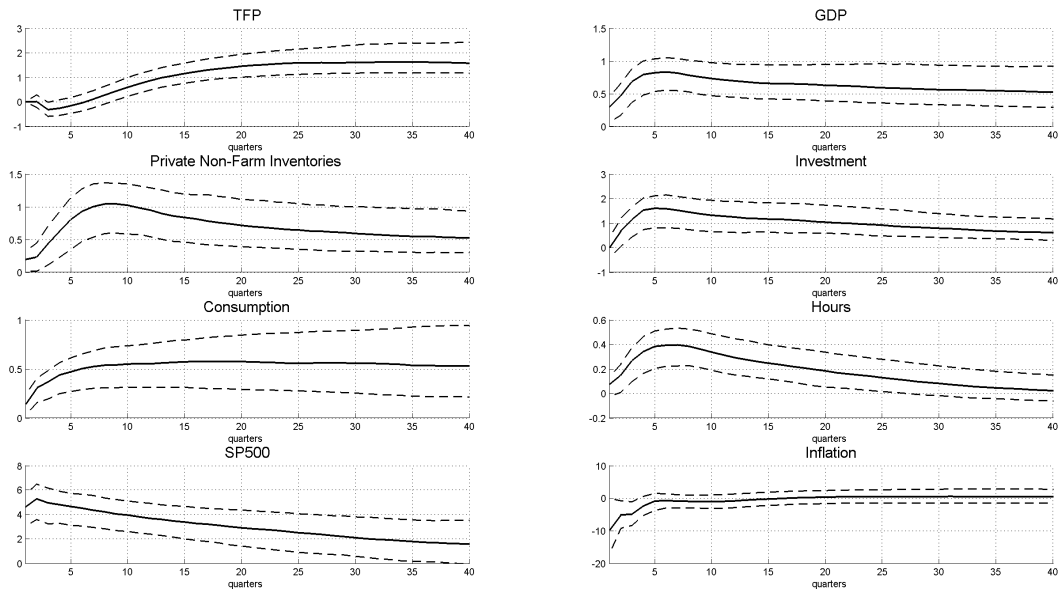


Figure 3: **IRF to TFP news shock. Sample 1948Q1-2018Q2.** The solid line is the median and the dashed lines are the 16% and 84% posterior bands generated from the posterior distribution of VAR parameters. The units of the vertical axes are percentage deviations.

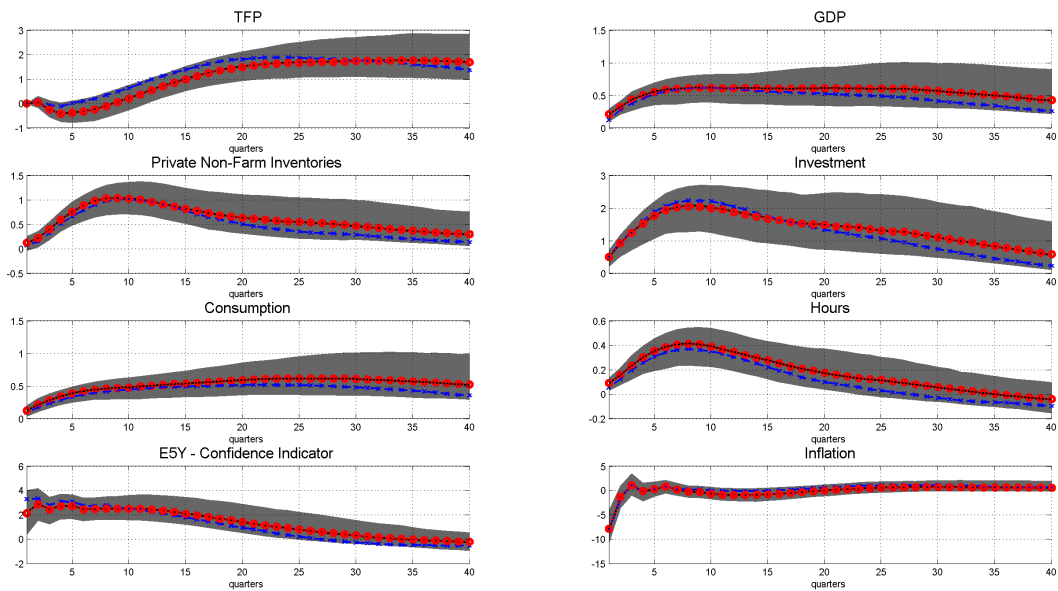


Figure 4: **IRF to TFP news shock. Sample 1983Q1-2018Q2.** The black solid line is the median response identified using the Max-share method. The shaded gray areas are the corresponding 16% and 84% posterior bands generated from the posterior distribution of VAR parameters. The blue line with crosses (red line with circles) is the median response identified using the Barsky and Sims (2011) (Forni et al. (2014)) methodology. The units of the vertical axes are percentage deviations.

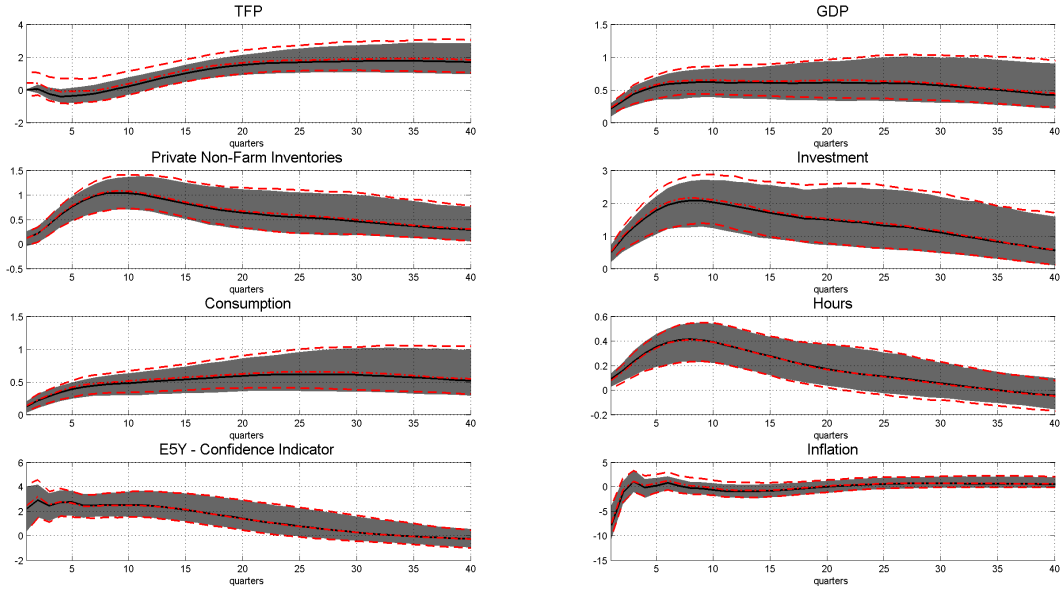


Figure 5: **IRF to TFP news shock**. Sample 1983Q1-2018Q2. The black solid (red dash-dotted) line is the median response identified using the Max-share (Kurmann and Sims (2016)) method. The shaded gray areas (dashed red lines) are the corresponding 16% and 84% posterior bands generated from the posterior distribution of VAR parameters. The units of the vertical axes are percentage deviations.

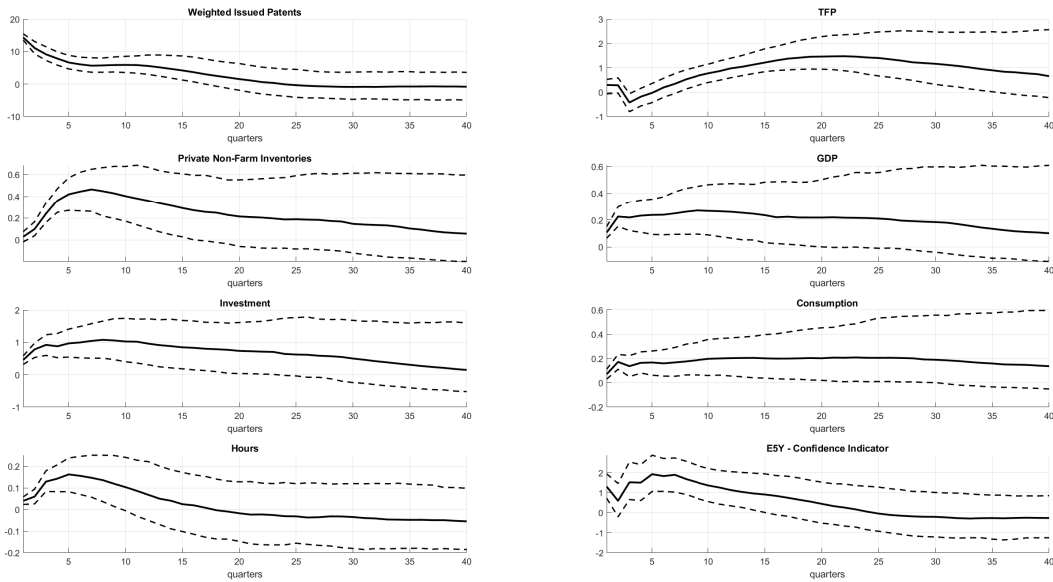


Figure 6: **IRF to patent based TFP news shock**. Sample 1983Q1-2010Q4. The black solid (dash-dotted) line is the median (16% and 84% posterior bands) response identified using the value weighted patent based identification as in Cascardi-Garcia and Vucotic (2019). Posterior bands are generated from the posterior distribution of VAR parameters. The units of the vertical axes are percentage deviations.

Table 1: Prior and Posterior Distributions

Parameter	Description	Prior Distribution			Posterior Distribution		
		Distribution	Mean	Std. dev.	Mean	10%	90%
Shocks: Persistence							
ρ_b	Preference	Beta	0.5	0.2	0.5281	0.5216	0.5364
ρ_μ	Marginal efficiency of investment	Beta	0.5	0.2	0.9997	0.9995	0.9999
ρ_g	Government spending	Beta	0.5	0.2	0.9552	0.9194	0.9287
ρ_a	TFP growth	Beta	0.5	0.2	0.4395	0.3798	0.5025
ρ_v	IST growth	Beta	0.5	0.2	0.6343	0.5555	0.7173
Shocks: Volatilities							
σ_b	Preference	Inv Gamma	0.5	2*	0.3177	0.1298	0.5160
σ_μ	Marginal efficiency of investment	Inv Gamma	0.5	2*	0.8943	0.1856	1.3684
σ_μ^4	MEI. 4Q ahead news	Inv Gamma	0.289	2*	1.3817	0.9850	1.8498
σ_μ^8	MEI. 8Q ahead news	Inv Gamma	0.289	2*	0.2860	0.0681	0.5308
σ_μ^{12}	MEI. 12Q ahead news	Inv Gamma	0.289	2*	0.3644	0.0966	0.6623
σ_g	Government spending	Inv Gamma	0.5	2*	0.2615	0.1450	0.3772
σ_g^4	Gov. spending. 4Q ahead news	Inv Gamma	0.289	2*	0.4545	0.1026	0.8695
σ_g^8	Gov. spending. 8Q ahead news	Inv Gamma	0.289	2*	0.2581	0.0681	0.5098
σ_g^{12}	Gov. spending. 12Q ahead news	Inv Gamma	0.289	2*	3.0040	2.7129	3.3181
σ_a	TFP growth	Inv Gamma	0.5	2*	0.6382	0.5778	0.7072
σ_a^4	TFP growth. 4Q ahead news	Inv Gamma	0.289	2*	0.1458	0.0861	0.2177
σ_a^8	TFP growth. 8Q ahead news	Inv Gamma	0.289	2*	0.1360	0.0723	0.1959
σ_a^{12}	TFP growth. 12Q ahead news	Inv Gamma	0.289	2*	0.6294	0.5419	0.7248
σ_v	IST growth	Inv Gamma	0.5	2*	0.3357	0.1652	0.4781
σ_v^4	IST growth. 4Q ahead news	Inv Gamma	0.289	2*	0.6004	0.4435	0.7898
σ_v^8	IST growth. 8Q ahead news	Inv Gamma	0.289	2*	0.1664	0.0797	0.2557
σ_v^{12}	IST growth. 12Q ahead news	Inv Gamma	0.289	2*	0.3769	0.2352	0.5091

Notes. The posterior distribution of parameters is evaluated numerically using the random walk Metropolis-Hastings algorithm. We simulate the posterior using a sample of 500,000 draws and discard the first 100,000 of the draws.